First-principles calculations of lattice-strained core-shell nanocrystals

K. H. Khoo,[1,*] J. T. Arantes,[2] James R. Chelikowsky,[3] and G. M. Dalpian[4]

[1]*Department of Materials Science and Engineering, Institute of High Performance Computing, Singapore 138632, Singapore*

[2]*Centro de Engenharia, Modelagem e Ciencias Sociais Aplicadas (CECS), Universidade Federal do ABC, Santo André, São Paulo, Brazil*

[3]*Center for Computational Materials, Institute for Computational Engineering and Sciences, Departments of Physics and Chemical Engineering, University of Texas, Austin, Texas 78712, USA*

[4]*Centro de Ciencias Naturais e Humanas (CCNH), Universidade Federal do ABC, Santo André, São Paulo, Brazil*

(Received 28 December 2010; revised manuscript received 5 April 2011; published 5 August 2011)

We have examined the properties of CdS-ZnS and ZnS-CdS core-shell nanocrystals over a range of shell thicknesses using a real-space pseudopotential-density functional theory approach. The effect of structural relaxation was shown to be important as it leads to significant changes in the band-gap and frontier orbital localizations. It was also predicted that strains at the core-shell interface are only affected by addition of the first few shell layers, with subsequent layers producing small changes in the strain configuration. This strain saturation gives rise to a "thin" shell regime in which both confinement and strain effects contribute to the evolution of the band gap and a "thick" shell regime in which band-gap variations from bulk values are strongly dependent on confinement effects but approximately constant with respect to strain.

DOI: 10.1103/PhysRevB.84.075311 PACS number(s): 65.80.−g, 31.15.A−, 81.05.Dz

I. INTRODUCTION

Semiconducting core-shell nanocrystals consist of an interior core region composed of one material and an outer passivating shell composed of a larger band-gap material. By varying the chemistry and thickness of each region, one can tune these nanocrystals to possess a wide range of properties, leading to applications in diverse areas such as optoelectronics,[1] biolabeling and sensing,[2] light-emitting diodes,[3] solar cells,[4] photovoltaic materials,[5] spintronics,[6,7] and lasers[8] using different growth techniques.[9–13] This is achieved by controlling the extent of quantum confinement and the nature of electronic and structural mismatch at the core-shell interface.

Predicting the localization of the highest-occupied (HOMO) and lowest-unoccupied molecular orbitals (LUMO) in core-shell nanocrystals has important implications for device applications. Depending on the band alignment of the core and shell materials, electrons and holes can be localized in the same material or staggered across core and shell regions, forming what are known as type-I and type-II heterostructures, respectively. To first order, we expect the localization of these charges to be similar to that of bulk heterostructures. However, owing to quantum confinement, both valence band maximum (VBM) and conduction band minimum (CBM) of nanocrystals will shift in energy, leading to changes in the band offset and band gap. As the energy shift varies inversely with the band effective mass, we expect the unoccupied states to be more strongly affected by changes in core-shell thickness than occupied ones. Another important effect that can modify the band gap and band offset configuration is the structural change induced by lattice mismatch between core and shell materials. These effects are especially important when the difference in lattice constant is large. Recently, epitaxial growth of a compressive shell onto a soft nanocrystalline core with a lattice mismatch of ∼14% has been achieved experimentally.[14] The low dimensionality and large surface-to-volume ratio enables the growth of lattice mismatched shell layers without introducing any defects or dislocations, as evidenced by x-ray diffraction data. The resulting strains coupled with quantum confinement effects have led to a type-I to type-II heterostructure transition with an increasing number of shell layers, accompanied by a large change in the optical gap.[14] This work highlights the importance of lattice strain in core-shell nanostructures.

Previously, there have been numerous theoretical studies on core-shell nanocrystals using a variety of numerical approaches, including the continuum effective mass and k·p method,[8,15–18] the empirical tight-binding method,[19–21] as well as the semiempirical pseudopotential method.[22,23] The effective mass k·p method might have problems treating nanocrystals containing a few monolayers, while bulk-like parameters within the tight-binding approximation might have transferability issues for small nanocrystals. The semiempirical pseudopotential method is a charge-patching method that yields reliable electronic properties of nanostructures from first principles. However, structural relaxation in this technique is based on a valence force field, and this might have limited applicability in treating small core-shell structures with a large lattice mismatch, as their properties deviate significantly from the bulk.

Here, we perform first-principles pseudopotential density functional theory (DFT) calculations on the normal CdS(core)-ZnS(shell) nanocrystals and also the inverted ZnS(core)-CdS(shell) nanocrystals, where the band gap of the shell material is less than that of the core. DFT is an appropriate level of theory for this problem as it is capable of capturing quantum confinement and lattice strain effects without any fitting parameters. A well-known issue with DFT is that it tends to underestimate band gaps, but this is not a problem here since we are more interested in the trends and physical origin of the band-gap changes and not so much the actual value of the gap.

Earlier interest in CdS-ZnS nanocrystals stems from its ability to emit blue light (below 480 nm) with superior brightness, color purity, and color tunability.[24–26] In addition, there is

also a 7% difference between the lattice constants of CdS and ZnS, allowing us to study the effects of lattice mismatch on the properties of core-shell nanocrystals. Specifically we seek to understand, as a function of shell thickness, structural changes at the core-shell interface, the variation of the HOMO-LUMO gap, and band offsets as well as HOMO-LUMO localizations. We would also like to compare the electronic properties of these systems before and after structural relaxation to assess the importance of lattice strain.

II. METHODOLOGY

Our calculations are based on an *ab initio* DFT formalism in which wave functions and potentials are represented on a uniform real-space grid and spatial derivatives are obtained by finite differencing.[27] This representation is complete, and convergence can be attained simply by decreasing the grid spacing. The boundary conditions are determined by setting the wave function to zero outside a spherical domain centered on the nanocrystal, with the domain radius chosen to be 3 Å larger than the nanocrystal radius. Tests have shown this criterion to converge energy eigenvalues to within 0.001 eV. The real-space formalism is also convenient for treating localized systems, as there is no implicit assumption of periodicity, and one avoids the problem of spurious interactions between the system and its replicated images. Ionic cores are represented using norm-conserving pseudopotentials with valence configurations $5s^25p^0$, $4s^24p^0$, and $3s^23p^4$ for Cd, Zn, and S atoms, respectively.[28] It has been shown that the *d*-electrons of Zn and Cd are relatively inert in this system, and they can be frozen into the pseudopotential core after core corrections have been taken into account.[29] A grid spacing of 0.5 a.u. was used for all calculations, and geometries were optimized using a force component cutoff of 0.004 Ry/a.u. The exchange-correlation energy and potential were evaluated using the local density approximation.[30] In addition, an improved algorithm known as the Chebyshev-filtered subspace iteration technique was used to solve the self-consistent Kohn-Sham equations, as it reduces the time-to-solution by at least an order of magnitude compared to standard eigensolvers. Details of this method have been published elsewhere.[31,32]

The unrelaxed core-shell nanocrystals were generated by cutting a spherical region from bulk zinc-blende material centered on a cation atom, giving rise to a structure with T_d symmetry.[33] The core of our nanocrystal has a diameter of about 1.2 nm and contains 35 atoms. We have done calculations for both CdS-ZnS and ZnS-CdS nanocrystals containing one, two, and three atomic shell layers, corresponding to nanocrystals containing 247, 453, and 933 atoms with diameters 1.8, 2.2, and 2.8 nm, respectively, as shown in Fig. 1. These nanocrystals were saturated by placing pseudohydrogen atoms at the surface to avoid the formation of dangling bonds,[34] as these bonds might generate gap states that would interfere in our results.[35] We have also performed calculations using our DFT method for bulk CdS (ZnS) and obtained equilibrium bond lengths of 2.53 Å (2.29 Å) and band gaps of 1.52 eV (2.60 eV).

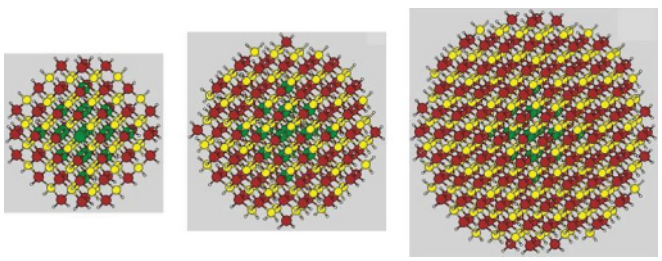

FIG. 1. (Color online) Ball-and-stick models of CdS-ZnS core-shell nanocrystals containing one to three shell layers around a 1.2-nm CdS core. Cd (green), Zn (red), S (yellow), and H (white).

III. RESULTS AND DISCUSSION

We compare the properties of relaxed and nonrelaxed CdS-ZnS core-shell nanocrystals to assess the importance of geometry optimization in these systems. For nonrelaxed nanocrystals, both CdS and ZnS bond lengths are set to the bulk CdS value (2.53 Å), as both VBM and CBM are known to reside in CdS for bulk CdS-ZnS heterostructures.[36] Only the pseudohydrogen atoms used for saturation are allowed to go to their minimum energy positions. This analysis is similar to that undertaken in a recent study on semiconducting core-shell nanowires.[37] It should also be noted that the choice of a fixed bond-length configuration for the nonrelaxed state serves as a reference state and introduces artificial stress into the nanocrystal.

In Fig. 2, we plot the density of states projected onto shells of different radii from the nanocrystal center. Results for relaxed nanocrystals are presented in Figs. 2(a)–2(c) and Fig. 2(d) is for the nonrelaxed nanocrystal having two shell layers. These plots give us information about the radial localization of every state in the system.

The radially projected density of states (PDOS) for the nonrelaxed CdS-ZnS nanocrystal having two shell layers is plotted in Fig. 2(d). It is clear from this plot that the wave function density of the HOMO state is localized in the core region, while that of the LUMO is in the shell region. This can also be seen from the core localization factors W_{core}, defined as the integral of wave function squared inside the core region, being 52% for the HOMO and 19% for the LUMO. A similar analysis carried out for other nonrelaxed CdS-ZnS nanocrystals having different shell thicknesses gives similar HOMO and LUMO localizations. The main effect of increasing the number of shell layers is that the HOMO-LUMO gap decreases, owing to decreasing quantum confinement. Our calculations yield energy gaps of 2.82 eV, 2.31 eV, and 1.92 eV for nanocrystals having one, two, and three shell layers, respectively. If one neglects the effects of geometry optimization on the electronic structure, it might be concluded that the CdS-ZnS nanocrystals demonstrates type-II behavior, with the HOMO and LUMO staggered across the core and shell regions and the HOMO-LUMO gap decreasing by 0.90 eV, going from a shell thickness of one to three layers.

However, once lattice relaxation is taken into consideration, the properties of these nanocrystals change dramatically. For the CdS-ZnS nanocrystal containing two shell layers, the average CdS bond length decreases to 2.47 Å due to compression by the ZnS shell, while the average ZnS bond length becomes 2.32 Å. It is also clear from Fig. 2(b) that after geometry optimization, the LUMO localization changes from

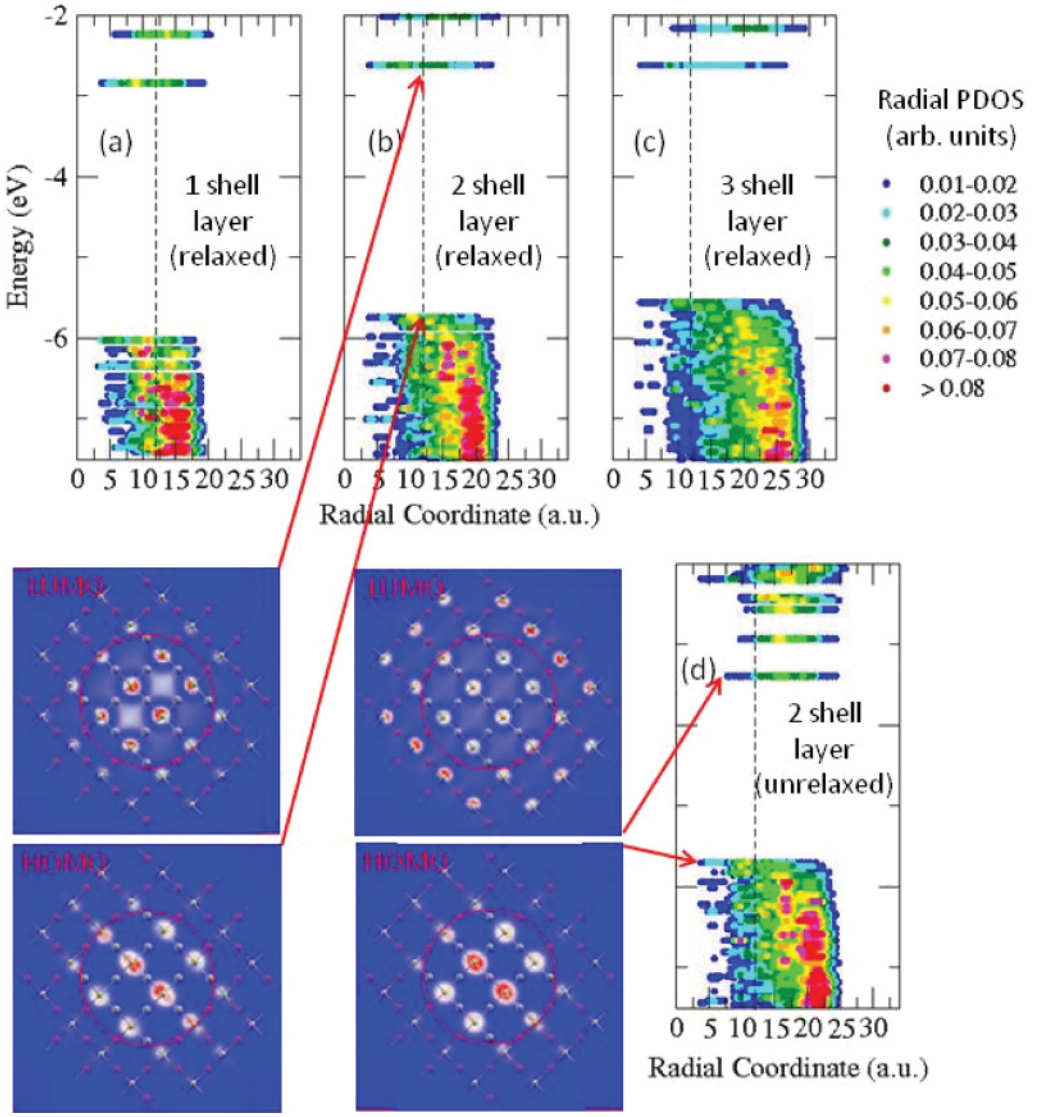

FIG. 2. (Color online) Radially PDOS of fully relaxed CdS-ZnS nanocrystals (2a to 2c) and nonrelaxed CdS-ZnS nanocrystal having two shell layers (2d). Dashed lines indicate the radial position of the core-shell interface. Panels are cross-sectional HOMO and LUMO density plots through nanocrystal center, and red circle denotes core-shell interface.

shell-like to corelike (W_{core} of LUMO increases from 19% to 52%), showing that this system exhibits type-I behavior if structural relaxation is considered. Accompanying this change is a large increase in the HOMO-LUMO gap from 2.31 eV to 3.13 eV. To explain these observations, we recall that in II-VI semiconductors, occupied states close to the gap are lowered in energy, while unoccupied states are raised in energy by isotropic lattice compression. Also, the unoccupied states are more affected by strain than occupied states owing to their more delocalized nature. Thus the compression of the CdS core and the large contraction in the ZnS shell causes a large increase in the band gap, with most of the contribution coming from shifts of unoccupied levels. Using the isotropic bulk deformation potentials $a_{CdS} = -2.27$ eV and $a_{ZnS} = -4.24$ eV,[38] we give an estimate for the energy shift of the lowest unoccupied CdS level as 0.16 eV and that of ZnS as 1.15 eV, neglecting shifts in the occupied levels. The fact that the shift of the ZnS unoccupied level is almost an electron volt more than that of the CdS level explains the change in localization of the LUMO from shell to core.

For the case of the inverted ZnS(core)-CdS(shell) nanocrystals, similar arguments apply. The radial PDOS for the nonrelaxed (bond length 2.53 Å) ZnS-CdS nanocrystal having two shell layers is plotted in Fig. 3(d). It can be seen that the LUMO is corelike ($W_{core} \sim 52\%$), and the HOMO is shell-like ($W_{core} \sim 10\%$), exhibiting type-II heterostructure behavior with a HOMO-LUMO gap of 2.31 eV. Our calculations show that the nonrelaxed ZnS-CdS nanocrystals, having one and three shell layers, exhibit similar type-II behavior and possess HOMO-LUMO gaps of 2.56 eV and 2.07 eV, respectively. Upon structural relaxation, the average CdS bond length in the shell region stays close to the bulk CdS value (2.54 Å) while that in the ZnS core region contracts to 2.43 Å. This pushes the unoccupied ZnS levels up in energy while keeping the CdS levels stationary, resulting in a shift of LUMO weight from the ZnS core to the CdS shell and a corresponding drop of W_{core}

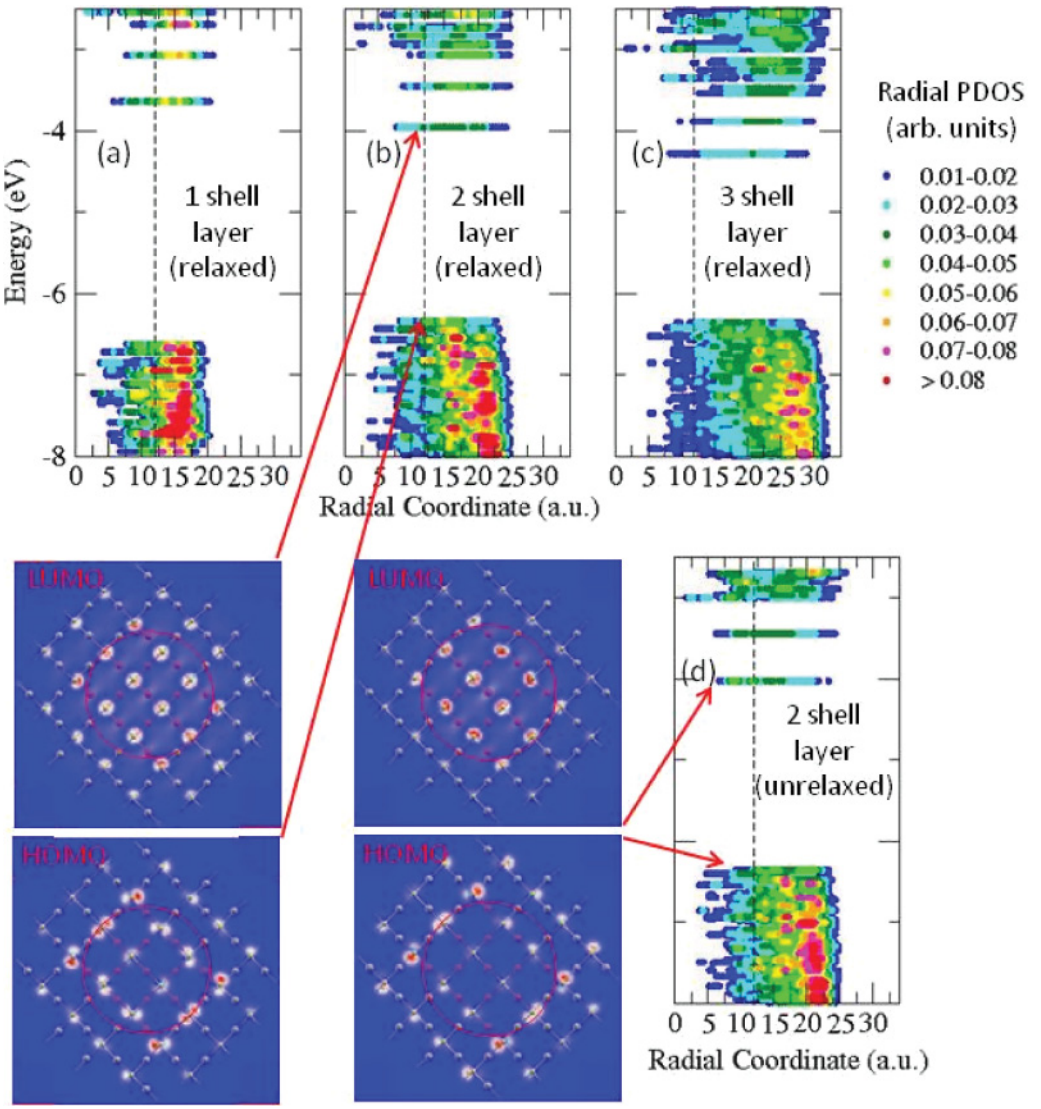

FIG. 3. (Color online) Radially PDOS of fully relaxed ZnS-CdS nanocrystals (3a to 3c) and nonrelaxed ZnS-CdS nanocrystal having two shell layers (3d). Dashed lines indicate the radial position of the core-shell interface. Panels are cross-sectional HOMO and LUMO density plots through nanocrystal center, and red circle denotes core-shell interface.

from 52% to 12% (see Fig. 3(b)). Accompanying this change of type-II to type-I behavior is a small increase in the band gap from 2.31 eV to 2.38 eV. The gap increase is small in this case because the lowest unoccupied CdS level starts out close to the LUMO in the nonrelaxed nanocrystal, and it remains largely unaffected by geometry optimization. Once the empty ZnS level is raised above this CdS state, it becomes the new LUMO and pins the value of the HOMO-LUMO gap.

It is clear from the above discussion that the inclusion of structural relaxation is very important in the study of CdS-ZnS core-shell nanocrystals. They may induce qualitative changes to the localization of the HOMO and LUMO and produce

TABLE I. Average bond lengths and bond-length strains (in brackets) in the core and shell regions and the HOMO-LUMO gap for CdS-ZnS and ZnS-CdS core-shell nanocrystals over range of shell thicknesses.

Core-shell	No. of shell layers	Average core bond length	Average shell bond length	E_g (eV)
CdS/ZnS	1	2.526 Å (−0.16%)	2.362 Å (3.14%)	3.19
	2	2.468 Å (−2.45%)	2.316 Å (1.13%)	3.13
	3	2.457 Å (−2.89%)	2.311 Å (0.92%)	2.94
ZnS/CdS	1	2.361 Å (3.10%)	2.508 Å (−0.87%)	2.98
	2	2.431 Å (6.16%)	2.546 Å (0.63%)	2.38
	3	2.446 Å (6.81%)	2.540 Å (0.40%)	2.08

changes in the size of the HOMO-LUMO gap. We consider the properties of fully relaxed CdS-ZnS core-shell nanocrystals as a function of shell thickness. Listed in Table I are the average bond lengths and bond-length strains (relative to bulk DFT values) in the core and shell regions along with the HOMO-LUMO gaps.

For the CdS-ZnS nanocrystal having one shell layer, the average bond length in the core region is close to the calculated bulk CdS value while that in the shell is increased relative to the calculated bulk ZnS value, because of stretching by the CdS core. Upon adding the second shell layer, the average bond lengths in the CdS core and ZnS shell decrease by 0.058 Å (−2.3% strain) and 0.046 Å (−2.0% strain), respectively, owing to the compressive influence of the additional ZnS layer. Accompanying this change is a small decrease of the HOMO-LUMO gap E_g from 3.19 eV to 3.13 eV. In going from two to three shell layers, the structural changes become much smaller, with the average bond lengths in the core and shell regions decreasing by only 0.011 Å (−0.4% strain) and 0.005 Å (−0.2% strain), respectively. However, the band-gap change in this case is larger, from 3.13 eV to 2.94 eV. The fact that the bond-length changes decay rapidly indicates that strain effects due to lattice mismatch are rapidly saturated as a function of shell thickness. This can also be seen by plotting the bond lengths as a function of distance from the nanocrystal center, as shown in Fig. 4(a).

Instead of being a continuously changing variable, the bond lengths change abruptly at the interface, and there is significantly less variation throughout the rest of the nanocrystal. The addition of a third shell layer only has a small impact on existing bond lengths in the two-shell-layer nanocrystal. It can also be seen that bond lengths in the shell region more than an atomic layer away from the core-shell interface are close to their unstrained bulk DFT values.

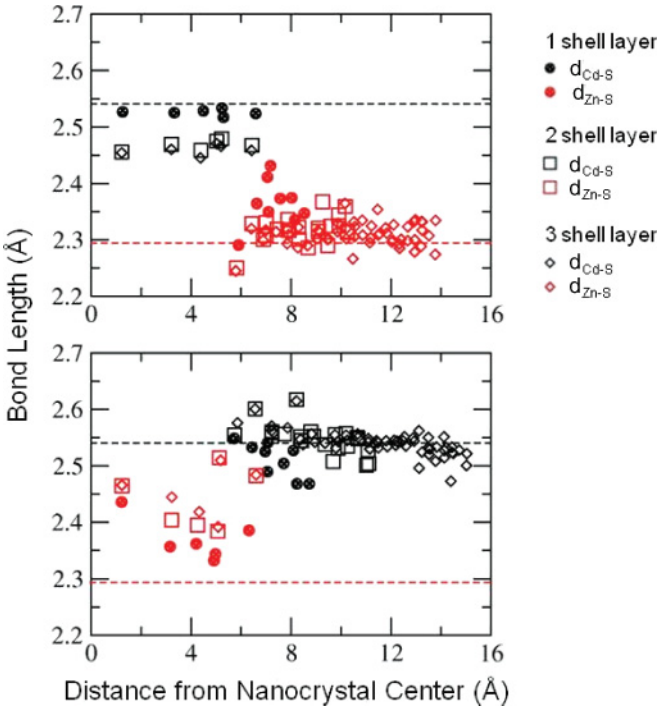

FIG. 4. (Color online) Bond lengths as a function of distance from nanocrystal center for (a) CdS-ZnS and (b) ZnS-CdS nanocrystals having different shell thicknesses. Dashed lines indicate bulk DFT bond-length values.

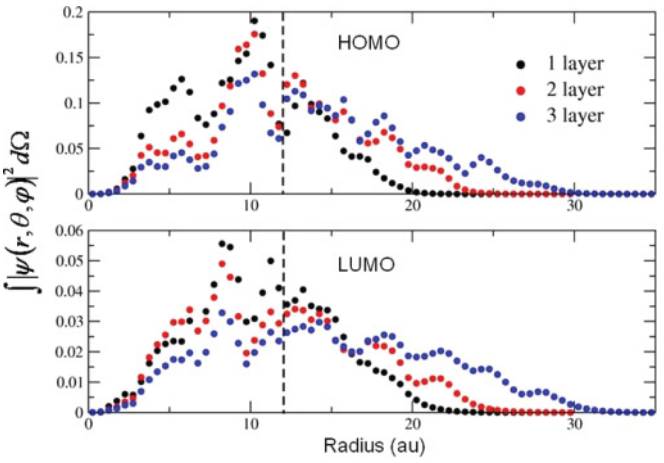

FIG. 5. (Color online) Radial distribution of modulus wave function squared for HOMO and LUMO of CdS-ZnS nanocrystals. Dashed line demarcates boundary between core and shell regions.

We investigate the dependence of the HOMO-LUMO gap with increasing shell thickness. The band gap changes by only −0.06 eV upon adding the second shell layer, but this change becomes appreciably larger at −0.19 eV for the addition of the third shell layer. To understand this peculiar behavior, we look at the two main factors controlling the size of the HOMO-LUMO gap, quantum confinement and lattice strain. From Figs. 2(a) to 2(c), it is clear that the system exhibits type-I behavior with the HOMO and LUMO states localized in the CdS core region, independent of shell thickness. Naively, one might expect increases in the shell thickness to have no effect on the quantum confinement of these frontier orbitals. However, the energy gap exhibits a decreasing trend, indicative of a reduction in quantum confinement. To explain these results, we plot the radial distribution of the modulus wave function squared for both HOMO and LUMO in Fig. 5. Even though a large proportion of the wave function weight is in the core region, there is also significant wave function density in the shell region of the nanocrystals. Because of this spillover, increasing the width of the shell region does give rise to less confined wave functions, as clearly illustrated in Fig. 5, leading to a decreased band gap.

Apart from quantum confinement, lattice strain also has a strong influence on the band gap as demonstrated earlier in the paper. On adding the second shell layer, the core region becomes compressed, and this should lead to an increase in the band gap as a result of the negative deformation potential of CdS. This is offset by a reduction in quantum confinement due to an increase in the shell thickness. The net result is a small decrease in the band gap by 0.06 eV. However, for the addition of the third shell layer, it is clear from Fig. 5 that there is a reduction in quantum confinement, but the bond lengths in the core remain fairly constant. The reduction in the HOMO-LUMO gap is significantly larger as the gap reduction due to reduced confinement effects is unopposed by any further core compression.

For the inverted ZnS-CdS nanocrystal having one shell layer, the CdS bond length is close to its bulk DFT value, and that of ZnS is strained by 3.1%. As the second shell layer is added, the average bond length in the ZnS core is increased by 0.070 Å, a consequence of the tensile stress imposed by the CdS shell layers, and that of the CdS shell is increased by 0.038 Å. These changes correspond to strain increases of 3.1% for ZnS and 1.5% for CdS. This is accompanied by a large decrease in the energy gap from 2.98 eV to 2.38 eV. In going from two to three shell layers, the structural changes become much smaller with the average bond lengths in the core region increasing by only 0.015 Å (0.7% strain) and that in the shell region decreasing by 0.006 Å (−0.2% strain). In this case, the band-gap change is correspondingly smaller, decreasing from 2.38 eV to 2.08 eV. As with the case of CdS-ZnS nanocrystals, the bond-length changes are only significant upon adding the first two shell layers, indicating that strain effects are quickly saturated with increasing shell thickness. This can also be seen in the plot of bond lengths vs radial distance (Fig. 4(b)), where we see little change in bond lengths on adding the third shell layer.

The variation of the HOMO-LUMO gap in the inverted ZnS-CdS nanocrystal is markedly different from that of the normal CdS-ZnS nanocrystal, with the band gap changing much more rapidly at smaller shell thicknesses (from one to two shell layers). This behavior can again be understood by considering the interplay between confinement and strain effects. Similar to the normal core-shell nanocrystals, it can be seen in Figs. 3(a) to 3(c) that the inverted nanocrystals exhibit type-I behavior. However, for this case, the HOMO and LUMO reside in the shell region. Thus increasing the shell thickness reduces the impact of quantum confinement and tends to decrease the HOMO-LUMO gap. In addition, adding more CdS shell layers partially offsets the influence of the ZnS core on the shell, thus raising the average shell bond length. Because of the negative deformation potential of CdS, this also decreases the band gap. Thus the strain and confinement effects reinforce each other to give rise to a large band-gap change on adding the second shell layer ($\Delta E_g = -0.60$ eV). However, when the third shell layer is added, the bond-length changes are small. The only contribution to band-gap change comes from a reduction in quantum confinement, leading to a smaller decrease in E_g.

From the above discussion, we see that there is a "thin" shell regime (one to two shell layers), where lattice-mismatch strains contribute as much to changes in the HOMO-LUMO gap as confinement effects with increasing shell thickness. This leads to very small band-gap changes in normal core-shell nanocrystals as strain and confinement effects tend to cancel out and large decreases in band gap for inverted core-shell nanocrystals as these effects reinforce each other. In the "thick" shell regime, where strains are saturated relative to increasing shell thicknesses (three or more shell layers), only confinement effects dominate to give qualitatively similar trends in band-gap changes for both normal and inverted core-shell nanocrystals.

IV. CONCLUSIONS

To summarize, we have investigated the structural and electronic properties of normal CdS-ZnS and inverted ZnS-CdS core-shell nanocrystals as a function of shell thickness using pseudopotential density functional theory calculations. It was found that geometry optimization in these nanostructures is very important and can lead to substantial changes in the HOMO-LUMO gap as well as qualitative changes in the localization of frontier orbitals. In addition, strains due to lattice mismatch rapidly saturate to fixed values as a function of shell thickness. This leads to a "thin" shell regime in which both confinement and strain effects contribute significantly to band-gap changes with increasing shell thickness and a "thick" shell regime in which band-gap variations from bulk values are strongly dependent on confinement effects, but approximately constant with respect to strain. Thus the variation of the HOMO-LUMO gap in normal CdS-ZnS nanocrystals is qualitatively different from that of inverted ZnS-CdS nanocrystals for thin shells, and the trend converges once the nanocrystal shells are sufficiently thick.

ACKNOWLEDGMENTS

We would like to acknowledge support from the National Science Foundation under grant DMR-09-41645 and the US Department of Energy, Office of Basic Energy Sciences and Office of Advanced Scientific Computing Research under grants DE-FG02-06ER15760 on nanostructures and DE-SC000187 on algorithms, respectively. Computational resources were provided by the National Energy Research Scientific Computing Center and the Texas Advanced Computing Center. The work in Brazil was supported by FAPESP, CAPES and CNPq.

*khookh@ihpc.a-star.edu.sg

[1] S. A. Empedocles and M. G. Bawendi, Science **278**, 2114 (1997).
[2] M. Bruchez, M. Moronne, P. Gin, S. Weiss, and A. P. Alivisatos, Science **281**, 2013 (1998).
[3] S. Coe, W.-K. Woo, M. Bawendi, and V. Bulovic, Nature **420**, 800 (2002).
[4] W. U. Huynh, J. J. Dittmer, and A. P. Alivisatos, Science **295**, 2425 (2002).
[5] D. Gross, A. S. Susha, T. A. Klar, E. Da Como, A. L. Rogach, and J. Feldmann, Nano Lett. **8**, 1482 (2008).
[6] W. K. Liu, K. M. Whitaker, K. R. Kittilstved, and D. R. Gamelin, J. Am. Chem. Soc. **128**, 3910 (2006).
[7] Y. A. Yang, O. Chen, A. Angerhofer, and Y. C. Cao, J. Am. Chem. Soc. **128**, 12428 (2006).
[8] S. A. Ivanov, A. Piryatinski, J. Nanda, S. Tretiak, K. R. Zavadil, W. O. Wallace, D. Werder, and V. I. Klimov, J. Am. Chem. Soc. **129**, 11708 (2007).
[9] C. Ricolleau, L. Audinet, M. Gandais, and T. Gacoin, Thin Solid Films **336**, 213 (1998).
[10] D. V. Talapin, I. Mekis, S. Gotzinger, A. Kornowski, O. Benson, and H. Weller, J. Phys. Chem. B **108**, 18826 (2004).

[11]P. Lommens, K. Lambert, F. Loncke, D. De Muynck, T. Balkan, F. Vanhaecke, H. Vrielinck, F. Callens, and Z. Hens, ChemPhysChem **9**, 484 (2008).
[12]U. T. D. Thuy, N. Q. Liem, D. X. Thanh, M. Protiere, and P. Reiss, Appl. Phys. Lett. **91**, 241908 (2007).
[13]T.-T. Han, Y. Fu, J. Wu, Y. Yue, and N. Dai, J. Phys. D Appl. Phys. **41**, 115104 (2008).
[14]A. M. Smith, A. M. Mohs, and S. Nie, Nat. Nanotechnol. **4**, 56 (2009).
[15]D. Schooss, A. Mews, A. Eychmuller, and H. Weller, Phys. Rev. B **49**, 17072 (1994).
[16]J. Berezovsky, M. Ouyang, F. Meier, D. D. Awschalom, D. Battaglia, and X. Peng, Phys. Rev. B **71**, 081309R (2005).
[17]V. Mlinar, M. Tadic, B. Partoens, and F. M. Peeters, Phys. Rev. B **71**, 205305 (2005).
[18]E. P. Pokatilov, V. A. Fonoberov, V. M. Fomin, and J. T. Devreese, Phys. Rev. B **64**, 245329 (2001).
[19]S. Pokrant and K. B. Whaley, Eur. Phys. J. D **6**, 255 (1999).
[20]R.-H. Xie, G. W. Bryant, S. Lee, and W. Jaskolski, Phys. Rev. B **65**, 235306 (2002).
[21]J. Perez-Conde and A. K. Bhattacharjee, Phys. Rev. B **67**, 235303 (2003).
[22]J. Schrier and L.-W. Wang, Phys. Rev. B **73**, 245332 (2006).
[23]J. Li and L.-W. Wang, Appl. Phys. Lett. **84**, 3648 (2004).
[24]J. S. Steckel, J. P. Zimmer, S. Coe-Sullivan, N. E. Stott, V. Bulovic, and M. G. Bawendi, Angew. Chem. Int. Ed. **43**, 2154 (2004).
[25]M. Protiere and P. Reiss, Nanoscale Res. Lett. **1**, 62 (2006).
[26]D. Chen, F. Zhao, H. Qi, M. Rutherford, and X. Peng, Chem. Mater. **22**, 1437 (2010).
[27]J. R. Chelikowsky, N. Troullier, K. Wu, and Y. Saad, Phys. Rev. B **50**, 11355 (1994); J. R. Chelikowsky, J. Phys. D **33**, R33 (2000); L. Kronik, A. Makmal, M. L. Tiago, M. M. G. Alemany, M. Jain, X. Huang, Y. Saad, and J. R. Chelikowsky, Phys. Stat. Sol. **243**, 1063 (2006).
[28]N. Troullier and J. L. Martins, Phys. Rev. B **43**, 1993 (1991).
[29]S. G. Louie, S. Froyen, and M. L. Cohen, Phys. Rev. B **26**, 1738 (1982).
[30]D. M. Ceperley and B. J. Alder, Phys. Rev. Lett. **45**, 566 (1980).
[31]Y. Zhou, Y. Saad, M. L. Tiago, and J. R. Chelikowsky, Phys. Rev. E **74**, 066704 (2006).
[32]K. H. Khoo, M. Kim, G. Schofield, and J. R. Chelikowsky, Phys. Rev. B **82**, 064201 (2010).
[33]G. M. Dalpian, M. L. Tiago, M. L. del Puerto, and J. R. Chelikowsky, Nano Lett. **6**, 501 (2006).
[34]X. Y. Huang, E. Lindgren, and J. R. Chelikowsky, Phys. Rev. B **71**, 165328 (2005).
[35]A. L. Schoenhalz, J. T. Arantes, A. Fazzio, and G. M. Dalpian, Appl. Phys. Lett. **94**, 162503 (2009).
[36]S.-H. Wei and A. Zunger, Appl. Phys. Lett. **72**, 2011 (1998).
[37]S. Y. Yang, D. Prendergast, and J. B. Neaton, Nano Lett. **10**, 3156 (2010).
[38]R. Said, A. Qteish, and N. Meskini, J. Phys. Condens. Matter **10**, 8703 (1998).